

The Effects of Alpha and Beta [70]fullerene Derivatives as Electron Transporting Materials in Perovskite Solar Cells

Edison Castro,^{a†*} Olivia Fernandez-Delgado,^{a†} Albert Artigas,^b Gerardo Zavala,^a Fang Liu,^c Antonio Moreno-Vicente,^d Antonio Rodríguez-Forteza,^d José D Velazquez,^{a,e} X-Y. Zhu,^c Josep M. Poblet,^d and Luis Echegoyen^{a*}

^a Department of Chemistry, University of Texas at El Paso, 500 West University Avenue, El Paso, TX 79968, United States

^b Institut de Química Computacional i Catàlisi (IQCC), Department de Química, Universitat de Girona, 17003 Girona, Catalonia, Spain.

^c Department of Chemistry, Columbia University, New York, New York 10027, United States

^d Departament de Química Física i Inorgànica, Universitat Rovira i Virgili, Marcel·lí Domingo 1, 43007, Tarragona (Spain)

^e Departamento de Química, Facultad de Ciencias Naturales y Exactas, Universidad del Valle, A.A. 25360 Cali, Colombia

KEYWORDS: fullerene derivatives, thiophene, Bingel adducts, electron transporting materials, perovskite solar cells.

Abstract

In this work, two new C₇₀ isomers, α and β bis(2-(thiophen-2-yl)ethyl)-C₇₀-fullerene mono-adducts (DTC₇₀), were synthesized, characterized and used as electron transporting materials (ETMs) in perovskite solar cells (PSCs). Our results show that the α isomer improves both the J_{sc} and FF values of the devices based on this derivative, when comparing to the β -isomer and phenyl-C₇₀-butyric acid methyl ester (PC₇₁BM) used as control. Devices based on α -DTC₇₀ achieved a power conversion efficiency (PCE) of 15.88%, which is higher than that observed with PC₇₁BM (15.15%).

Introduction

In the past few years, the development of organic-inorganic hybrid perovskite solar cells (PSCs) has received special attention because of the fast improvement in terms of their PCE, from 3.8% in 2009 to 25.2% in 2019,¹ easy fabrication procedures and low cost.^{2, 3} These materials are promising for the production of new devices with enhanced properties for commercial applications.⁴⁻¹⁰

Among the different device configurations, inverted p-i-n planar PSCs have emerged as a new alternative due to their simple device architecture and low temperature manufacturing processes, while still keeping considerably high performances.¹¹ Another advantage of planar inverted PSCs is their versatility regarding both the hole transporting materials (HTMs) and the ETMs.¹²⁻¹⁶ In this regard, fullerenes are considered the best ETMs in inverted PSCs because of their deep lying lowest unoccupied molecular orbital (LUMO) that match with the conduction band of the perovskite¹⁷ and their ability to accept up to six electrons.^{2, 18}

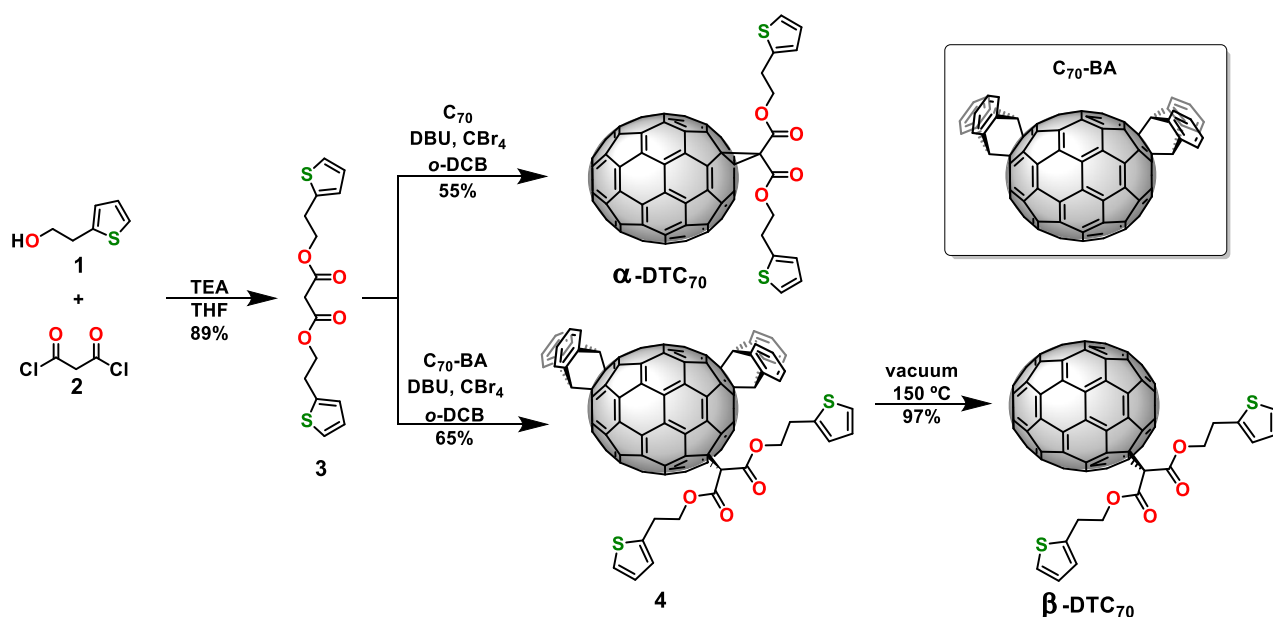
One of the most used fullerene derivatives in PSCs fabrication is the phenyl-C₆₀-butyric acid methyl ester (PC₆₁BM), but many other fullerenes have been successfully incorporated in PSCs.^{2, 19} It is worth noting that the function of fullerenes in PSCs is not only limited to accept and transport electrons. A wide variety of fullerene derivatives bearing different functional groups have been used with several purposes: as ETM compact layers, as interfacial modification layers, as additives, as cathode buffer layers and as double layers.^{2, 3, 19}

Charge recombination and hysteretic behaviour are some of the drawbacks that affect the performance of PSCs. Recently, it has been shown that the introduction of heteroatom-containing motifs on fullerene derivatives can effectively passivate the trap sites of the surface of the perovskite layer by interaction with undercoordinated Pb²⁺ cations.²⁰ As a result of this interaction, charge recombination and hysteresis can be suppressed, thus improving the overall photovoltaic performance.²⁰ It has been reported that fullerene derivatives passivate the trap sites present both, on the surface and the grain boundaries of the perovskite layer.^{21,}

On the other hand, functionalization of fullerenes has been widely studied to improve their solubility as well as their physical and optical properties.²²⁻²⁵ When functionalizing C₇₀, different isomers can be obtained, making the purification process difficult. Some of us have reported that the use of a α -[C₇₀]fulleropyrrolidine as the ETM outperforms the regioisomeric mixture. Such difference was attributed to the energy disorder provided by the different α , β and γ isomers present in the mixture. Similar outcomes were reported in other works.²⁶⁻²⁸ In general, the use of regioisomeric mixtures in photovoltaic devices often results in lower PCEs when compared to their corresponding pure isomers.^{20, 29-34} When comparing pure isomers vs regioisomeric mixtures, most of the research so far has focus mainly on the α -isomer, which are more easily prepared than their β counterparts. Recently, we have reported a very straight forward methodology to selectively synthesize pure C₇₀ β -isomers.³⁵ Additionally, we also reported that the introduction of thiophene moieties in the fullerene cage increases the interaction of the ETM and the perovskite layer, thus raising the photovoltaic performance. Here, we report the synthesis and characterization of the α and β bis(2-(thiophen-2-yl)ethyl)-C₇₀-fullerene (DTC₇₀) mono-adducts and studied their effects in PSCs when used as the ETMs.

Results and Discussion

The α -DTC₇₀ and β -DTC₇₀ (Scheme 1) fullerene derivatives were synthesized according to our previously reported methodology.^{35, 36} The α -DTC₇₀ isomer was prepared by a Bingel cyclopropanation reaction of malonate derivative **3** and fullerene C₇₀. The product was obtained with 55% yield after chromatographic purification. For the synthesis of the β -DTC₇₀ isomer, C₇₀ was first reacted with anthracene to yield the α -6- α' C₇₀-BA isomer, which was used as a template to direct the subsequent cyclopropanation reaction to the C_s-symmetric tris-adduct isomer (**4**). Retro Diels-Alder reaction of **4** resulted in the selective synthesis of the β -DTC₇₀ isomer with a 63% overall yield (see materials and methods for details). The pure compounds were characterized by means of ¹H-NMR and ¹³C-NMR spectroscopy, UV-Vis and matrix assisted laser desorption ionization-time of flight mass spectrometry (MALDI-TOF MS) (Figures S1-S10).



Scheme 1: Synthesis of α -DTC₇₀ and β -DTC₇₀.

Recently, we reported that the functionalization of C₆₀ with thiophene groups substantially improved their solubility in organic solvents such as chlorobenzene (CB), and PCE values higher than those of PC₆₁BM based-devices were obtained for C₆₀ thiophene derivatives-based devices. Additionally, devices fabricated with the compounds bearing the thiophene groups showed slower degradation, which was attributed to the specific interactions between the sulphur atoms present in the addend and the free lead cations from the surface of the perovskite layer.³⁶

The feasibility of the α -DTC₇₀ and β -DTC₇₀ compounds to be used in inverted PSCs as ETMs was anticipated by estimation of their HOMO-LUMO energy values from UV-vis and cyclic voltammetry (CV) (Figures S7 and S8). Both isomers exhibited electrochemical and chemical reversibility displayed by three well-defined and independent reduction and oxidation waves. The reduction onset potentials (E_{red}^{on}) for both isomers were estimated from the CV measurements using the equation $LUMO = -e(E_{red}^{on} + 4.8)$ (eV) and they are summarized in Table 1. The energy levels diagram in Figure 1a shows that the work function of the new derivatives matches with that of the perovskite. The two isomers exhibit deep enough HOMO values to block the holes and low LUMO values to allow the fast transport of electrons, which indicates that they can be used efficiently as ETMs in PSCs.

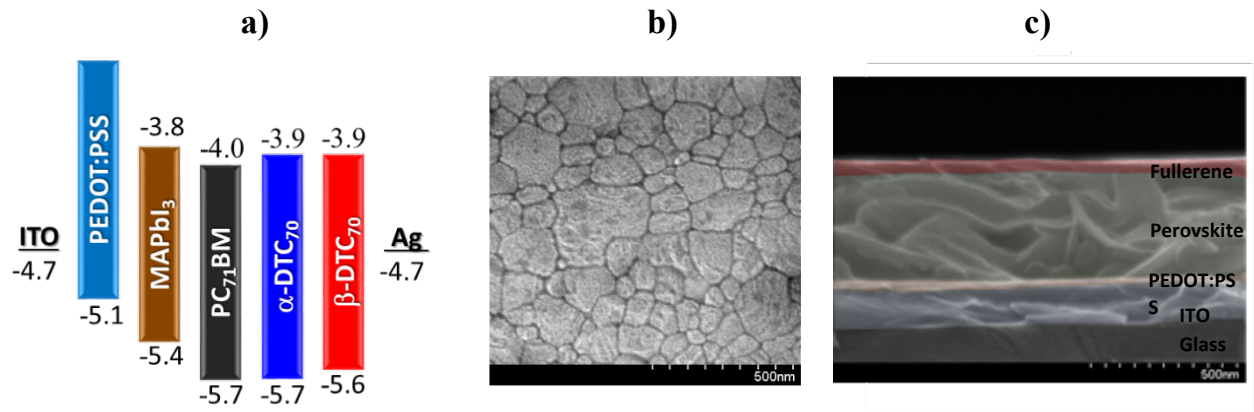


Figure 1 a) Energy levels diagram, PC₇₁BM values were taken from the literature,²⁰ b) surface SEM image of the perovskite layer and c) cross section SEM of the perovskite device.

Table 1. Optical bandgap, onset reduction and LUMO/HOMO energy levels of α-DTC₇₀ and β-DTC₇₀.

| Compound | λ_{abs} (nm) | E_g (eV) | $E_{\text{red}}^{\text{on}}$ (V) | LUMO (eV) | HOMO (eV) |
|---------------------|-----------------------------|------------|----------------------------------|-----------|-----------|
| α-DTC ₇₀ | 695 | 1.78 | -0.92 | -3.88 | -5.66 |
| β-DTC ₇₀ | 710 | 1.75 | -0.93 | -3.87 | -5.62 |

X-ray diffraction (XRD) was performed to characterize the formation of the perovskite layer. As observed in Figure S11 the perovskite is completely formed, as indicated by the characteristic diffraction planes 100, 112, 211, 202, 220, 310, 312, 322 that suggest the formation of a tetragonal phase perovskite.³⁷ To study the quality of the films, scanning electron microscopy (SEM) was recorded to investigate the morphology of the perovskite layer, which revealed homogeneity with no visible pin holes, and an average grain size of 200 nm (Figure 1b). The cross-section SEM (Figure 1c) measurements showed the indium tin oxide (ITO) transparent electrode (50 nm), poly(3,4-ethylenedioxythiophene):poly-styrene sulfonate (PEDOT: PSS) as hole transporting material (25 nm), perovskite active layer (300 nm), and the fullerene ETL(80 nm).

To study the performance of α -DTC₇₀ and β -DTC₇₀ as ETMs, PSCs planar devices with an inverted configuration (ITO/PEDOT:PSS/perovskite/ α -DTC₇₀ or β -DTC₇₀/Ag) were fabricated. (see materials and methods for fabrication details).

Current-voltage (J - V) curves for both isomers and PC₇₁BM as control were obtained under AM 1.5G irradiation (100 mW cm⁻²) in air. The photovoltaic parameters such as FF, J_{sc} , and V_{oc} are listed in Table 1. As shown in Figure 2 and Table 3 a maximum PCE value of 15.88% was achieved from devices based on α -DTC₇₀ whereas PCE values of 15.15% and 8.80% were obtained from PC₇₁BM and β -DTC₇₀ based devices, respectively. The J_{sc} and FF values were improved in the case of the α isomer, this is attributed to its high electron mobility and well solubility in dichlorobenzene, whereas in the case of the β isomer, it has been reported that the packing in the solid state is not as compact and efficient as compared to the α isomer, yielding to a lower photovoltaic performance.³⁸

Figure S12 shows the PCEs based on statistical histograms obtained from 25 devices. The average efficiencies for α -DTC₇₀, β -DTC₇₀ and PC₇₁BM based devices are 14.34% \pm 0.54%, 8.29 \pm 0.51% and 14.86% \pm 0.29, respectively, showing narrow margins for the three compounds, which is an indicative of the good performance reproducibility.

The J_{sc} values were also investigated by external quantum efficiency (EQE) as shown in Figure 2b. The values obtained from EQE were in concordance with the ones extracted from the J - V curves, which suggest that the high J_{sc} and FF values for the α -DTC₇₀ isomer can be related to a better ability to extract electrons in the visible spectrum window. Also, we can conclude from the spectra that α -DTC₇₀ can efficiently convert more than 80% of the incident photons into electrons in the visible range when compared to β -DTC₇₀ and PC₇₁BM.

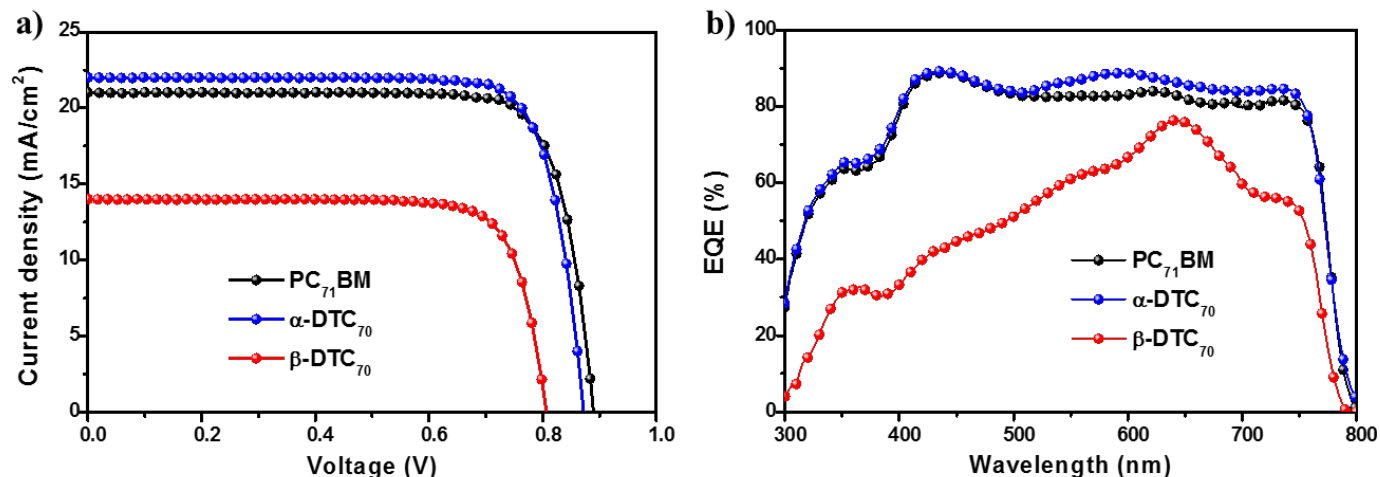


Figure 2 a) J - V curves and b) EQE spectra of PSCs fabricated with α -DTC₇₀, β -DTC₇₀ and PC₇₁BM as ETMs.

Table 3. Summary of device performance. The calculated J_{sc} values were obtained from the EQE curves. Values in parentheses represent the best PCEs measured.

| Compound | Calculated J_{sc} (mA/cm ²) | J_{sc} (mA/cm ²) | V_{oc} (V) | FF (%) | PCE (%) |
|-----------------------------|--|--------------------------------|--------------|--------|--------------------|
| PC ₇₁ BM | 20.94 | 21.01 | 0.89 | 0.81 | 14.86±0.29 (15.15) |
| α -DTC ₇₀ | 21.95 | 22.00 | 0.87 | 0.83 | 14.34±0.54 (15.88) |
| β -DTC ₇₀ | 13.97 | 14.09 | 0.81 | 0.77 | 8.29±0.51 (8.80) |

Steady state photoluminescence (SSPL) measurement and time resolve photoluminescence (TRPL) were performed to demonstrate that the α and β derivatives are good at extracting electrons, passivating the perovskite layer, and decreasing the electron-hole recombination. These measurements were collected from devices with the structure glass/perovskite and glass/perovskite/fullerene.

Figure 2a shows that the perovskite layer exhibited a high PL signal, as the result of electron-hole recombination events, while perovskite/fullerene devices showed a very efficient quenching of the photoluminescence, a clear indication of the ability of these compounds to

reduce this recombination process. These results were very similar to those obtained from perovskite/PC₇₁BM devices. To study the kinetics of the electron-hole recombination, TRPL was also collected by monitoring the emission peak (780 nm) as a function of time. Figure 3b, shows that the decay time for α -DTC₇₀ is faster than that of PC₇₁BM and β -DTC₇₀, which indicates that electrons are being more efficiently transferred from the perovskite layer to α -DTC₇₀ than β -DTC₇₀ and PC₇₁BM. This result could explain the devices performance since a faster decay time indicates a faster injection of electrons into the ETL, thus, overcoming the recombination processes.

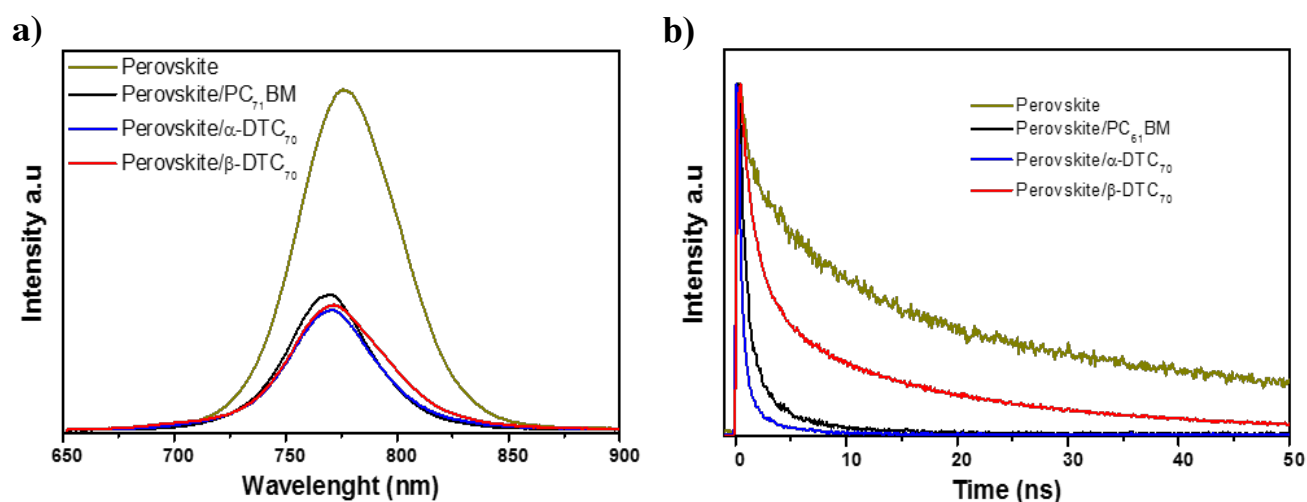


Figure 3 a) SSPL and b) TRPL of the perovskite, perovskite/ α -DTC₇₀, perovskite/ β -DTC₇₀ and perovskite/PC₇₁BM layers.

Stability studies were performed on encapsulated devices under 50% humidity at ambient conditions. The devices remained stable up to 7 days in which the ones containing α -DTC₇₀ retained 80% of their initial PCE compared to 42% and 40% for β -DTC₇₀ and PC₇₁BM, respectively. As shown in the Figure 4, α -DTC₇₀ devices showed comparatively better photostability than β -DTC₇₀ and PC₇₁BM devices, which can be attributed to better packing in the solid state, thus allowing higher environmental resistance.

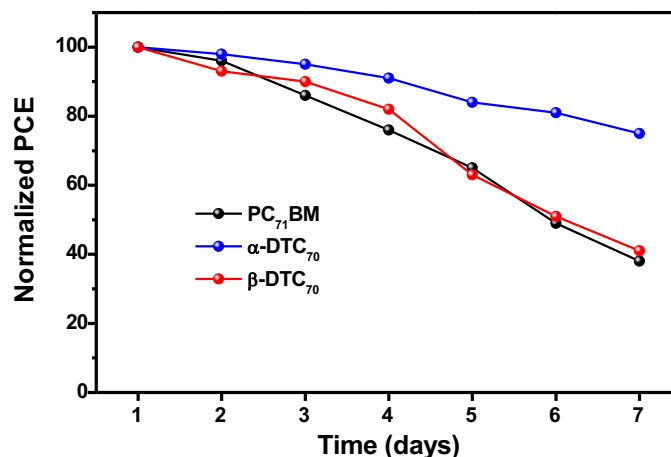


Figure 4 Stability Studies of the PSCs fabricated with α -DTC₇₀, β -DTC₇₀ and PC₇₁BM as the ETMs.

To better understand the interaction between α -DTC₇₀ and β -DTC₇₀ fullerene adducts and the perovskite surface, we have performed periodic density functional theory (DFT) calculations. Previous studies on PC₆₁BM-like derivatives showed that these compounds interact with the surface via the fullerene and also via the addend.³⁷ The latter occurs through a direct interaction between the Pb²⁺ ions and carbonyl or ester substituents. In the C₇₀ adducts, the situation is similar but the lower symmetry of the C₇₀ cage increases somewhat the complexity because of the higher number of regioisomers involved and the possible different orientations of the addends with respect to the surface. Mono functionalization of C₇₀ affords preferentially C₁-C₂ adducts (α type regioisomers), whereas the second most reactive bond is C₅-C₆ giving a β type regioisomers.³⁹ As shown in Figure 5, α and β isomers exhibit different local symmetry, with α isomer showing a symmetry plane through the C₁-C₂ (red) bond. It is worth mentioning that for β -DTC₇₀ regioisomers, two different adsorption modes on the perovskite surface are possible depending on the way the C=O groups of the malonate are attached to the Pb sites of the surface. We call β -1 mode when the C=O group on the side of the pentagon is the one bonded to the Pb atom, whereas the β -2 mode corresponds to the situation when the attached C=O is the one on the side of the hexagon (Figure 5).

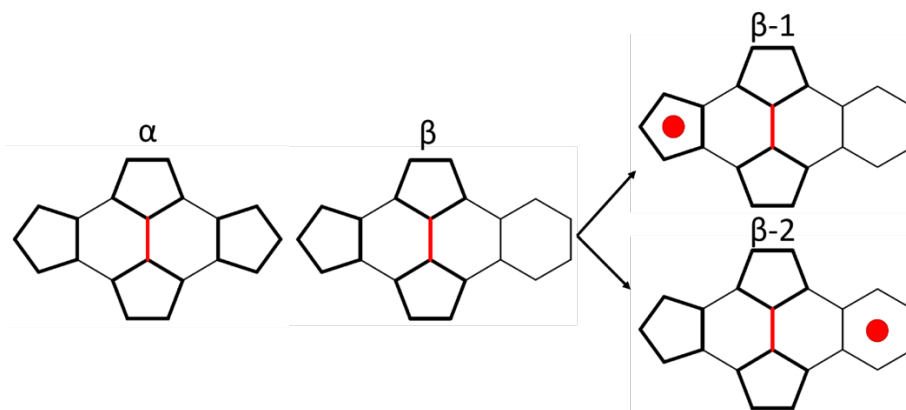


Figure 5. α and β motifs for the [6,6] Bingel adducts of C_{70} . The red line represents the substituted carbon-carbon bond. For a representation of β_1 and β_2 isomers see Figure S13.

Table 4 collects adsorption energies and structural data for several orientations of fullerene adducts deposited on the perovskite surface. Initially, we have analyzed in detail the different orientations of a pristine C_{70} in contact with the surface. We have two fullerene alignments, cap and equatorial and three surface sites, hollow, top and bridge. Figure S14 summarizes the adsorption energies computed for the different pristine C_{70} structures, which range between -1.07 eV and -1.81 eV. The optimal alignment corresponds to the fullerene interacting with a hollow site through the poles. The second most stable orientation is the bridge-equatorial one with an adsorption energy of -1.59 eV, only 0.22 eV higher than the lowest in energy minimum. Indeed, for the α -DTC $_{70}$ adduct, we have found that the most exothermic adsorption energy occurs when the fullerene is interacting in a bridge site, as shown in Figure 6b.

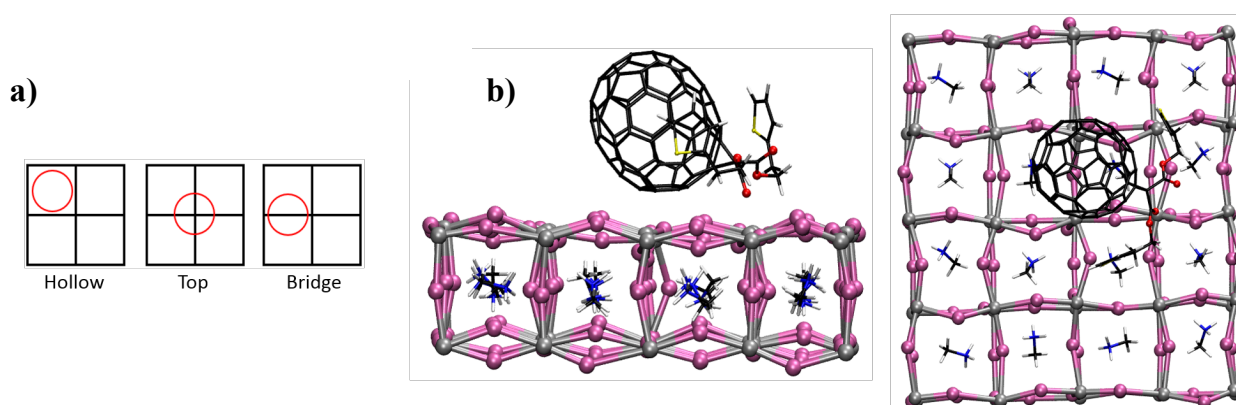


Figure 6. a) Schematic representation of three types of adsorption sites of the fullerene on the perovskite surface and b) two views of the lowest in energy structure (bridge isomer) for α -DTC $_{70}$.

The top and the hollow sites are less exothermic by 0.35 and 0.67 eV. The change in the fullerene orientation with respect to the pristine fullerene is due to the carbonyl-lead interaction that fixes the fullerene on the perovskite surface. The adsorption energies for the fullerene adducts are in general between 0.10 and 0.77 eV larger than in the pristine fullerene. This can be rationalized if we consider that the strong O–Pb²⁺ interactions easily overcome the loss of fullerene-surface interaction imposed by the addend constraints.

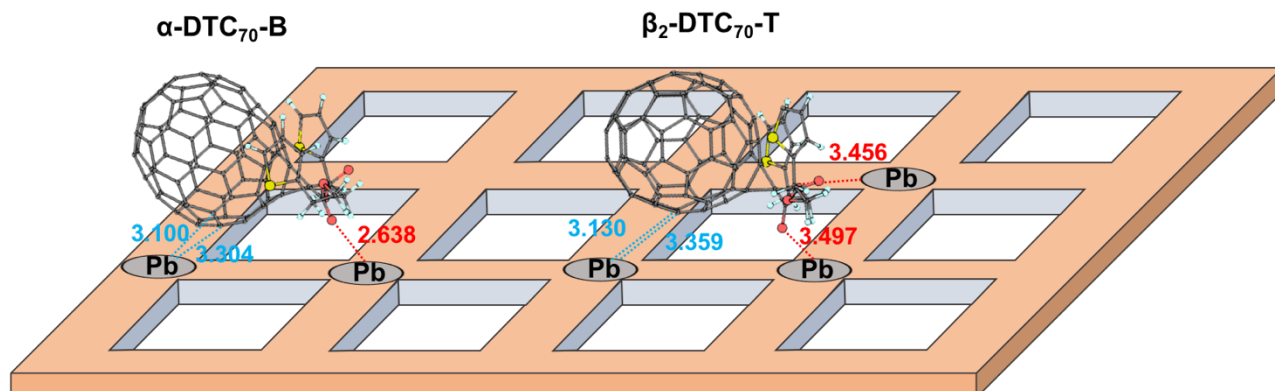


Figure 7. Schematic representation for the lowest in energy α -DTC₇₀ and β -DTC₇₀ adducts adsorbed on the MAPbI₃ surface. The values in red and cyan correspond to the shortest lead-fullerene and lead addend distances (in Å), respectively. A 3D view of the metal adduct contacts can be found in Figure S15.

Table 4. Adsorption energies and shortest distances for the different isomers of the fullerene adducts and adsorption sites.

| Isomer | E_{ads} ^{a)} | RE ^{b)} | $d_{\text{Pb-O}}$ ^{c)} | $d_{\text{Surf-C70}}$ ^{d)} |
|---|--------------------------------|------------------|---------------------------------|-------------------------------------|
| α -DTC ₇₀ -hollow | -1.90 | 0.67 | 2.869 | 3.138 < 3.226 < 3.411 |
| α -DTC ₇₀ -top | -2.23 | 0.35 | 2.615 | 3.226 < 3.516 < 3.742 |
| α -DTC ₇₀ -bridge | -2.36 | 0.22 | 2.638 | 3.100 < 3.304 < 3.679 |
| β ₁ -DTC ₇₀ -hollow | -2.54 | 0.04 | 2.655 | 3.393 < 3.405 < 3.776 |
| β ₁ -DTC ₇₀ -top | -2.43 | 0.15 | 2.709 | 3.175 < 3.394 < 3.640 |
| β ₁ -DTC ₇₀ -bridge | -2.54 | 0.04 | 2.689 | 3.284 < 3.346 < 3.795 |
| β ₂ -DTC ₇₀ -hollow | -2.01 | 0.57 | 2.857 | 3.315 < 3.338 < 3.528 |

| | | | | |
|---|-------|------|-------|-----------------------|
| β_2-DTC₇₀-top | -2.58 | 0.00 | 3.497 | 3.130 < 3.359 < 3.515 |
| β_2-DTC₇₀-bridge | -2.48 | 0.10 | 3.009 | 3.201 < 3.516 < 3.526 |

a) Adsorption energies in eV; b) relative energies with respect to β_2 -DTC₇₀-top. c) shortest Pb-O distance in Å; d) shortest contacts between the carbon atoms of the fullerene and the perovskite surface in Å.

A similar analysis was done for the β regioisomers, for which we have found three orientations of the fullerene on the surface in an energy range of only 0.04 eV. The most exothermic adsorption energies are displayed by two β_1 -DTC₇₀ adducts in hollow and bridge sites and one β_2 isomer in top. Indeed, β_2 -DTC₇₀-top corresponds to the adduct with the shortest carbon-lead distance (3.130 Å). In β_1 -DTC₇₀-bridge and β_1 -DTC₇₀-hollow sites, the fullerene is found at longer separations from the surface, but the loss of interaction is compensated by the stronger Pb-addend interactions, revealed by shorter Pb-O distances (Table 4). Due to the small energy differences, it is reasonable to believe that in our device the β_1 -DTC₇₀ isomers are occupying different adsorption sites on the perovskite surface.

The electronic structure of lead-halide perovskites has been recurrently analyzed by means of DFT calculations showing that the valence band is mainly formed of antibonding states derived from hybridizations of 5p orbitals of iodine and 6s orbitals of lead, while the conduction band is mainly constituted of empty 6p orbitals of lead.⁴⁰⁻⁴³ Given that the electron transfer from the excited perovskite to the fullerene empty orbitals has probably to involve the conduction band of the perovskite, we have analyzed the fullerene–lead contacts. In agreement with the experimental results, which, exhibits a higher efficiency for the α -DTC₇₀ isomer, Figure 7 shows that the shortest contacts are observed for this isomer. Nevertheless, the contact distances between carbon atoms and lead are not very different and likely other factors, such as fullerene adduct compactness and packing could be relevant in the electron-transport.

Conclusions

In conclusion, we have regioselectively synthesized new α - and β -C₇₀ fullerene derivatives by following our previously reported methodology. The new compounds were fully characterized and tested in inverted PSCs as ETMs. Our results show significant differences when compared to each other and to the PC₇₁BM control devices. The α -DTC₇₀ exhibited an enhancement of the overall

device performance with higher PCE, J_{sc} and FF values and a significantly improved ability to extract electrons as evidenced by PL. Additionally, the long term stability was also improved when devices were prepared with the α isomer, retaining 80% of the initial PCE for up to 7 days after fabrication. The effect of the two new C_{70} isomers when used as ETMs in PSCs was rationalized by DFT calculations.

Corresponding author

*eacastroportillo@utep.edu

*echegoyen@utep.edu

Author contribution

†These authors contributed equally.

Conflict of interest

There are no conflicts to declare.

Acknowledgements

Authors thank the US National Science Foundation (NSF) for generous support of this work under the NSF-PREM program DMR 1205302 and CHE-1801317. The Robert A. Welch Foundation is also gratefully acknowledged for an endowed chair to L. E. (Grant AH-0033). Research reported in this paper was supported by the National Institute of General Medical Sciences of the National Institutes of Health under linked Award Numbers RL5GM118969, TL4GM118971, and UL1GM118970. Authors also thank Spanish Ministry of Science (grant CTQ2017-87269-P), the Generalitat de Catalunya (grant 2017SGR629) and the URV for support. J.M.P. also thanks ICREA foundation for an ICREA ACADEMIA award. The content is solely the responsibility of the authors and does not necessarily represent the official views of the National Institutes of Health.

References

1. NREL, Best Research-Cell Efficiencies., <https://www.nrel.gov/pv/assets/pdfs/best-research-cell-efficiencies.20200218.pdf>, (accessed March, 2020, 2020).
2. E. Castro, J. Murillo, O. Fernandez-Delgado and L. Echegoyen, *J. Mater. Chem. C.*, 2018, **6**, 2635-2651.
3. Y. Fang, C. Bi, D. Wang and J. Huang, *ACS Energy Lett.*, 2017, **2**, 782-794.
4. M. A. Green, A. Ho-Baillie and H. J. Snaith, *Nat. Photonics*, 2014, **8**, 506.
5. M. Liu, M. B. Johnston and H. J. Snaith, *Nature*, 2013, **501**, 395.
6. M. D. McGehee, *Nat. Mater.*, 2014, **13**, 845.
7. A. Kojima, K. Teshima, Y. Shirai and T. Miyasaka, *J. Am. Chem. Soc.*, 2009, **131**, 6050-6051.
8. G. Xing, N. Mathews, S. Sun, S. S. Lim, Y. M. Lam, M. Grätzel, S. Mhaisalkar and T. C. Sum, *Science*, 2013, **342**, 344.
9. S. D. Stranks, G. E. Eperon, G. Grancini, C. Menelaou, M. J. P. Alcocer, T. Leijtens, L. M. Herz, A. Petrozza and H. J. Snaith, *Science*, 2013, **342**, 341.
10. C. Tian, E. Castro, T. Wang, G. Betancourt-Solis, G. Rodriguez and L. Echegoyen, *ACS Appl. Mater. Interfaces*, 2016, **8**, 31426-31432.
11. X. Liu, Y. Cheng, C. Liu, T. Zhang, N. Zhang, S. Zhang, J. Chen, Q. Xu, J. Ouyang and H. Gong, *Energy Environ. Sci.*, 2019, **12**, 1622-1633.
12. L. Tanghao, C. Ke, H. Qin, Z. Rui and G. Qihuang, *Adv. Energy Mater.*, 2016, **6**, 1600457.
13. E. H. Anaraki, A. Kermanpur, L. Steier, K. Domanski, T. Matsui, W. Tress, M. Saliba, A. Abate, M. Gratzel, A. Hagfeldt and J.-P. Correa-Baena, *Energy Environ. Sci.*, 2016, **9**, 3128-3134.
14. S. Yang, W. Fu, Z. Zhang, H. Chen and C.-Z. Li, *J. Mater. Chem. A*, 2017, **5**, 11462-11482.
15. H. Kim, K.-G. Lim and T.-W. Lee, *Energy Environ. Sci.*, 2016, **9**, 12-30.
16. L. Jiang, W. Gang, L. Kun, H. Xulin, Y. Qinyan, L. Cheng and M. Jun, *ChemPhysChem*, 2017, **18**, 617-625.
17. P. Schulz, E. Edri, S. Kirmayer, G. Hodes, D. Cahen and A. Kahn, *Energy Environ. Sci.*, 2014, **7**, 1377-1381.
18. L.-L. Deng, S.-Y. Xie and F. Gao, *Adv. Electron. Mater.*, 2017, DOI: 10.1002/aelm.201700435, 1700435.

19. T. Gatti, E. Menna, M. Meneghetti, M. Maggini, A. Petrozza and F. Lamberti, *Nano Energy*, 2017, **41**, 84-100.
20. E. Castro, G. Zavala, S. Seetharaman, F. D'Souza and L. Echegoyen, *J. Mater. Chem. A*, 2017, **5**, 19485-19490.
21. Y. Shao, Z. Xiao, C. Bi, Y. Yuan and J. Huang, *Nat. Comm.*, 2014, **5**, 5784.
22. C. Tian, E. Castro, G. Betancourt-Solis, Z.-A. Nan, O. Fernandez-Delgado, S. Jankuru and L. Echegoyen, *New J. Chem.*, 2018, **42**, 2896-2902.
23. A. a. B. Hirsch, M., *Front Matter*, GmbH & Co. KGaA: Weinheim, Germany, 2004.
24. H. Andreas, *Angew. Chem. Int. Ed.*, 1993, **32**, 1138-1141.
25. A. Hirsch, *Journal*, 2000, **8**, 125-126.
26. T. Umeyama and H. Imahori, *Acc. Chem. Res.*, 2019, **52**, 2046-2055.
27. F. Zhang, W. Shi, J. Luo, N. Pellet, C. Yi, X. Li, X. Zhao, T. J. S. Dennis, X. Li, S. Wang, Y. Xiao, S. M. Zakeeruddin, D. Bi and M. Grätzel, *Adv. Mater.*, 2017, **29**, 1606806.
28. E. Castro, G. Zavala, S. Seetharaman, F. D'Souza and L. Echegoyen, *J. Mater. Chem. A*, 2017, **5**, 19485-19490.
29. W. W. H. S. Wong, J.; White, J. M.; Seyler, H.; Zhang, B.; Jones, D. J.; Holmes, A. B., *Chem. Mater.* , 2014, **26**, 1686.
30. K. X. Sun, Z.; Lu, S.; Zajaczkowski, W.; Pisula, W.; Hanssen, E.; White, J. M.; Williamson, R. M.; Subbiah, J.; Ouyang, J.; Holmes, A. B.; Wong, W. W. H.; Jones, D. J., *Nat. Commun.* , 2015, **6**, 6013.
31. A. B. Mishra, P. , *Angew. Chem., Int. Ed.* , 2012, **51**, 2020.
32. Y. C. Sun, C.; Wang, H.; Li, Y. , *Adv. Energy Mater.* , 2012, **2**, 996.
33. M. W. Lenes, G.-J. A. H.; Kooistra, F. B.; Veenstra, S. C.; Hummelen, J. C.; Blom, P. W. M. , *Adv. Mater.* , 2008, **20**, 2116.
34. T. M. Umeyama, T.; Jakowetz, A. C.; Shibata, S.; Kurotobi, K.; Higashino, T.; Koganezawa, T.; Tsujimoto, M.; Gelinas, S.; Matsuda, W.; Seki, S.; Friend, R. H.; Imahori, H. , *Chem. Sci.* , 2017, **8**.
35. M. R. Cerón, E. Castro, V. S. P. K. Neti, P. W. Dunk and L. A. Echegoyen, *J. Org. Chem.*, 2017, **82**, 893-897.
36. E. Castro, O. Fernandez-Delgado, F. Arslan, G. Zavala, T. Yang, S. Seetharaman, F. Dsouza and L. Echegoyen, *New J. Chem.*, 2018, DOI: 10.1039/c8nj03067g.

37. O. Fernandez-Delgado, E. Castro, C. R. Ganivet, K. Fosnacht, F. Liu, T. Mates, Y. Liu, X. Wu and L. Echegoyen, *ACS Appl. Mater. Interfaces*, 2019, **11**, 34408-34415.
38. X.-X. Zhan, X. Zhang, S.-M. Dai, S.-H. Li, X.-Z. Lu, L.-L. Deng, S.-Y. Xie, R.-B. Huang and L.-S. Zheng, *Chem. Eur. J.*, 2016, **22**, 18709-18713.
39. M. B. Andreas Hirsch, *Fullerenes: chemistry and reactions*, Wiley-VCH Verlag GmbH & Co, Germany, 2005.
40. M. Caputo, N. Cefarin, A. Radivo, N. Demitri, L. Gigli, J. R. Plaisier, M. Panighel, G. Di Santo, S. Moretti, A. Giglia, M. Polentarutti, F. De Angelis, E. Mosconi, P. Umari, M. Tormen and A. Goldoni, *Sci. Rep.*, 2019, **9**, 15159.
41. E. Mosconi, P. Umari and F. De Angelis, *Phys. Chem. Chem. Phys.*, 2016, **18**, 27158-27164.
42. L. M. Herz, *Annu. Rev. Phys. Chem.*, 2016, **67**, 65-89.
43. V. Blum, R. Gehrke, F. Hanke, P. Havu, V. Havu, X. Ren, K. Reuter and M. Scheffler, *Comput. Phys. Commun.*, 2009, **180**, 2175-2196.